J Mater Sci: Mater Electron (2021) 32:22155–22167

The effects of Bi substitution for Sn on mechanical properties of Sn-based lead-free solders

Mehdi Raza[1], Lee Shewchenko[1], Ayodele Olofinjana[1,*], Damon Kent[1], Jitendra Mata[2], and Rezwanul Haque[1]

[1] School of Science, Technology and Engineering, University of the Sunshine Coast, Sippy Downs, QLD 4556, Australia
[2] Australian Centre for Neutron Scattering, Australian Nuclear Science and Technology Organisation, Lucas Heights, NSW 2234, Australia

Received: 15 June 2021
Accepted: 21 July 2021
Published online: 2 August 2021

ABSTRACT

Pb-free solders are gaining ground as the optimum choice for electrical interconnect materials, however, their higher melting temperature around 217 °C is still an issue that restricts wider adoption. The potential to employ Bi substitution for Sn to lower solder joint processing temperatures has been widely considered. In this work, the mechanical properties of eutectic SAC with gradually increasing Bi substitution up to 10 wt% Bi was studied. It is shown that fracture strength (σ_f) increases with Bi additions from 50 MPa plateauing at 60 MPa between 1.4 and 1.8% Bi which represents the limits of solid solution strengthening. Over this substitutional range, strain at fracture (ε_f) dropped from 30 to 10% which was also evidenced by smaller percentage reduction in area (%RA). The σ_f was nearly 80 MPa for 2% Bi increasing gradually with increasing Bi concentrations and peaking at 93 MPa for 7% Bi whilst maintaining 10% elongation at fracture. X-ray diffraction and DSC thermal studies suggests that the solubility limit of Bi in β-Sn (in the multicomponent SAC) is less than 2 wt% Bi. With the aid of small-angle neutron Scattering (SANS) and ultra-small-angle neutron scattering (USANS), it was found that the scattering intensity changes for alloys with Bi content in the range 0.8 – 1.5wt% compared to ternary SAC with less than 0.8% Bi at low scattering factors ($Q > 10^{-2}$ Å^{-1}) signifying microstructural differences at length scales of the order of 10–100 nm. There were no differences observed in scattering for alloy samples with more than 2 wt% Bi.

Address correspondence to E-mail: aolofinj@usc.edu.au

https://doi.org/10.1007/s10854-021-06691-y

1 Introduction

Emerging legislative requirements, from the implementation of Restriction of Hazardous Substances (RoHS) in electronic devices and the growth of consumerism requiring smaller and more functional products, have driven the development of new unleaded electrical interconnect materials [1]. The functionality and longevity of solder joints are characterised by their reliability in the field; therefore, the solder must use optimum physical and chemical properties to ensure robust interconnections. Despite having drawbacks like cost and durability considerations, the transition from conventional Sn–Pb eutectic alloys to Pb-free solder alloys is taking place at a fast pace. In recent years, considerable efforts [1–3] have been made to develop Pb-free alloys that match the operational performance of the traditional Sn–Pb eutectic solders. Concurrently, there is growing demand for soldering alloys that can service more demanding functional requirements in new small portable devices. The move to a cost-effective alternative to these solder systems involves incremental development of research involving reliable solder alloy material compositions, industrial process development, inventory clearance, and product certification. Different families of non-leaded solders are now commercially available and most of these are formulated around eutectic Sn-based systems.

It is of particular importance to understand the thermal characteristics of candidate alloys to inform their processing in manufacturing, especially for mounting and interconnecting of sensitive electronics [4]. The thermal fatigue reliability of SAC solders depends on the microstructural constituents. Though generally, the family of SAC are known to have good thermal fatigue, the near-eutectic commercial alloys SAC305 and SAC405 exhibit the best thermal fatigue properties [5]. Lower Ag content in SAC alloys results in an increased rate of particle coarsening during thermal cycling and therefore shorter lifetimes. It is found [5] that a higher density of Ag_3Sn precipitates decelerates the microstructural coarsening effect. To compensate for the loss of strength due to particle coarsening, alloys that provide solid solution strengthening and at higher concentration initiate a eutectic shift to provide the energy potential for off-eutectic freezing leading to formation of primary precipitates are considered desirable [6]. Additionally, the particle coarsening mechanism which accelerates failure in solder alloys has been attributed to temperature cycling-induced strain paired with thermal exposure at the higher end of the cycle [7]. Considering these critical reliability aspects, alloys with higher Ag content (> 3%wt) ternary SAC alloys with a eutectic around Sn-3.5Ag-0.9Cu (wt%) are selected for this research. These alloys exhibit melting properties that are considered the most promising to replace and match the properties of Sn–Pb solders. Some of the advantages of SAC alloys are ease of use, comparatively slow creep rate, whilst showing promising strength and ductility. SAC alloys show increased performance efficiency under thermal fatigue testing as the range of thermal cycling temperature reduces, outperforming Sn–Pb alloys under less severe cycling conditions [5, 7]. Commercially, they are available in near-eutectic compositions as SAC305 (Sn-3Ag-0.5Cu) and SAC405(Sn-4Ag-0.5Cu) and other far eutectic compositions with lower Ag contents to reduce cost. SAC solders have been documented to exhibit high resistance to mechanical vibration, impact, and creep at temperatures up to 150 °C, improving upon the thermomechanical properties of Sn–Pb [8]. However, eutectic SAC alloy has a melting point of 217.2 °C [6] approximately 34 °C higher than Sn–Pb which can limit their potential for broader application.

Substitution of another element into lead-free solders is a common method for improving thermal characteristics and achieving optimal properties. It has been demonstrated that the addition of Al_2O_3 nanoparticles to Sn-based Pb-free solder alloys improved wettability and mechanical properties by refining the microstructure through the nucleation effect of the nanoparticles [9]. SAC alloys generally have better corrosion resistance than lead-containing solders but recent work [10] suggests that corrosion properties can be improved by the addition of a quintenary component as an alloying element or addition of a small volume proportion of metallic oxide nanoparticles. Bismuth (Bi) due to its ability to lower the melting temperature of the solder, low cost relative to other materials, and low toxicity has become an attractive choice as an alloying component in lead-free solders. However, as the solid solubility limit of Bi in the Sn-Ag-based solder at room temperature is reported to be 4 wt%, higher levels of Bi could lead to precipitation of a pure Bi-phase [11, 12]. Although recent studies by Hu, et al. [13] suggests the functional limits of Bi substitution for Sn within SAC

solders occurs at approximately 3 wt% Bi, our preliminary work [14] indicated that much is left to be understood about the effects of Bi for more dilute and higher concentrations of Bi in SAC.

Interfacial reactions between the solder and the substrate occur during soldering lead to the formation of intermetallic compounds (IMCs). The formation of IMCs encourages the binding of the solder with the substrate. The brittle nature of large IMCs at the interface tends to be detrimental to the mechanical properties of the joint. This can be particularly observed in the case of solder alloys containing Bi which exhibit segregation of Bi at Cu/Cu_3Sn interfaces when soldered onto Cu substrates. Whilst the existence of IMCs indicates good wetting characteristics, the durability of solder devices can be impaired by excessive intermetallic layer development. It has been previously reported that 1%wt addition of Bi into the solder alloy can improve the wetting capability by inhibiting the excessive formation of IMCs during soldering and subsequent ageing processes [15–17]. Substitution of elements in SAC solders can affect interfacial reactions by altering the rate of growth of IMCs, creating reactive layers, and changing the properties of phases formed during these reactions. The eutectic phases formed during solidification of SACs are: β-Sn and the intermetallic phases Ag_3Sn and Cu_6Sn_5. These phases commonly exist in morphologies of Ag_3Sn plates, hollow hexagonal Cu_6Sn_5 needles, and non-faceted dendrites of β-Sn [18]. SAC alloys face difficulty in nucleating Sn solidification as a pro-eutectic phase due to exhibiting a high degree of undercooling. However, reaching a fully eutectic microstructure is difficult due to the potential for deviation from the equilibrium eutectic solidification. For example, during slow cooling increased undercooling of the SAC joints promotes the formation of undesirable pro-eutectic Ag_3Sn intermetallic which can coarsen and lead to embrittlement of the solder joint [19]. This means the time for cooling and diffusion of Ag and Sn should be shorter to inhibit the growth of Ag_3Sn. The intermix of microstructure from near equilibrium to metastable affects the mechanical properties of the soldered joint. There is still much to be understood on the role of Bi addition to SAC and the possible nanoscale microstructural changes for dilute (< 3%) Bi substitution in the SAC alloys. Small-angle neutron scattering and ultra-small-angle neutron scattering (SANS and USANS) experiments were conducted in this research to study the morphology of Bi precipitates in SAC-Bi alloys making it the first time these techniques were used to study structure across such a large length scale for SAC alloys with Bi substitution. This work is therefore aimed at exploring the effects of modification of SAC alloys with Bi to understand changes in the functional properties required in interconnecting of electronic components in new RoHS compliant devices.

2 Experimental

2.1 Alloy selection

SAC alloys with composition around the eutectic form the basis of the commercially available SAC305/405. To study the effects of Bi substitution on the functional properties it is appropriate to base our study on the eutectic composition Sn 95.6wt%-Ag3.5wt%-Cu0.9wt%. Therefore, we study the eutectic SAC with increasing levels of Bi substitution for Sn with 0.25% Bi increments up to 3wt%. Beyond 3 wt% Bi, the increments were increased and alloys containing 4, 7, and 10 wt% Bi were analysed to enable extrapolation of the changes in thermal and mechanical characteristics.

2.2 Preparation and casting of SAC-Bi alloys

Alloy compositions of SAC-Bi were determined proportionally by weight percentage with Bi substitution for Sn in the eutectic composition SAC-alloy series. The elemental makeup of each composition was weighed using granular, high purity Sn-99.99wt% chemically pure Ag-99.99wt% electrolytic oxygen-free Cu and Bi-99.99wt%. The alloy components were weighed into batches of 80 g and loaded into an alumina crucible. A mixture of LiCl/KCl at a molar ratio of 41.8/58.2 corresponding to the eutectic of the LiCl/KCl system as predicted by the thermodynamically calculated Phase diagram [20] was melted at 500 °C and was poured on the cold mixture of alloy component in the alumina crucible to form a protective flux on the alloy mixes before melting.

The alloy mixes covered by molten salt were finally fired to 600 °C in a muffle furnace during which the elemental component melted and the molten salt mixture formed a protective flux layer over the

molten alloy. The sequence of casting is illustrated in Fig. 1. The mixture was left in the furnace to equilibrate at 600 °C during which the molten salt flux protected the metallic melt from oxidation, as shown in Fig. 1. The melt was then stirred using a borosilicate glass rod to ensure uniformity in concentration and was given time to attain enough superheating before the casting procedure.

The crucible was then removed from the muffle furnace whilst the superheat kept both the alloy and salt mixtures molten during the casting process. The alloys were cast into 8 mm rods by vacuum action that sucked the molten alloy into borosilicate tubing, as illustrated in Fig. 1. The salt was eventually washed off under running water. The castings came out as rods attached to the remnant pool as illustrated in Fig. 2. All of the rods and the remnant melt pool came out with a metallic lustre finish (Fig. 2) demonstrating the effectiveness of the protective action of the molten salt mixture. The rods were then sectioned into samples for tensile testing, observation by scanning electron microscopy (SEM), and thermal analyses.

2.3 Thermal properties

The thermal characteristics were monitored for each sample followed by a NETZSCH 449 F3 Jupiter simultaneous thermal analyser (STA), using the

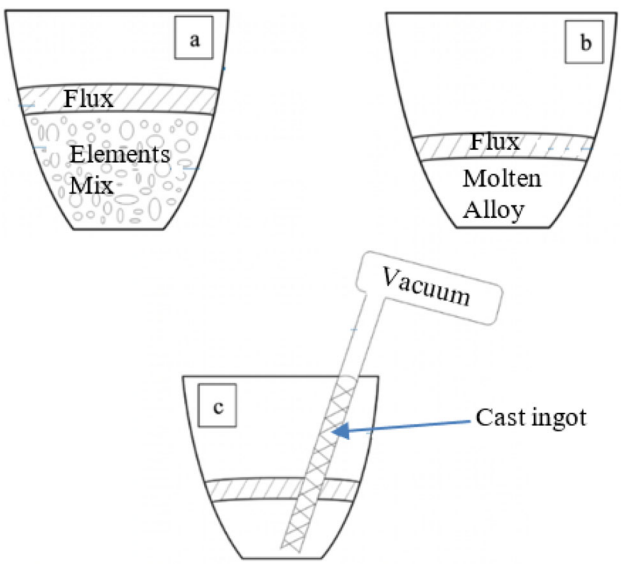

Fig. 1 Illustrative sketch of alloy making, and casting **a** Flux protection of element mix, **b** Molten alloy with flux protection, **c** Vacuum casting into borosilicate tubbing

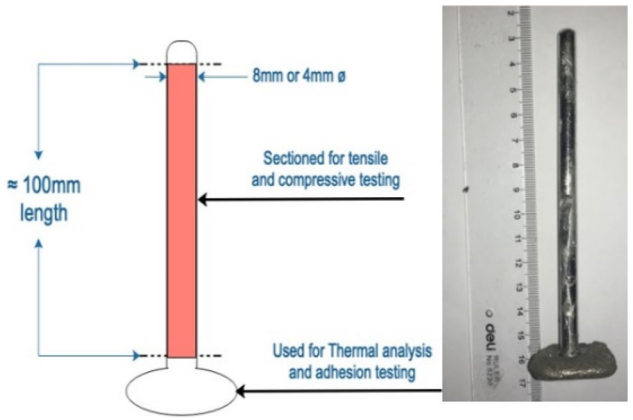

Fig. 2 As-cast alloy profile and sectioning for tests

differential scanning calorimeter (DSC) mode. Samples for DSC were weighed on an electronic balance with sensitivity ±0.1 0 mg. About 40 mg sample of each composition is loaded onto an alumina pan and subjected to thermal balance following the power energy difference to maintain the temperature of a sample and reference in an inert atmosphere of sweeping argon gas. The sample was subjected to a thermal program to heat slowly at 1 °C/min from room temperature to 400 °C and cooled to room temperature with the instrument fan-forced cooling. The melting observed in the heating cycle is used to characterise the thermal properties. The thermograms for heating and cooling cycles were compared to follow the extent of undercooling. The DSC instrument was programmed to normalise the effect of mass to present the DSC signal output in W/mg.

2.4 Tensile testing

Tensile testing was performed on the SAC-Bi series of alloys using samples obtained from the 8 mm diameter rod castings. Test samples were machined into a dog-bone profile, and the specific dimensions as illustrated in Fig. 3. The tensile tests were conducted on a Shimadzu UTM, where the test samples were pneumatically gripped at the jaws of the machine.

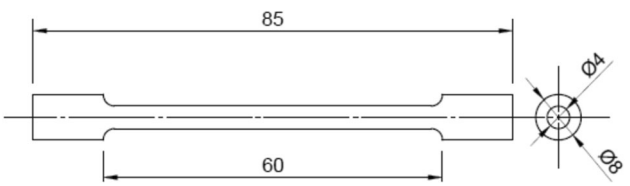

Fig. 3 Engineering drawing showing the dimensions in mm of tensile test samples

The tests were performed at a crosshead speed of 1 mm/min with load applied via a 100kN load cell. The tensile test data were collected via a physically attached extensometer with a gauge length of 50 mm. The raw data were collected as force–displacement data and were processed using spreadsheeting software into stress–strain data.

2.5 Scanning electron microscopy (SEM)

Scanning electron microscopy (SEM) was carried out on JEOL JSM-TT 100 operated with an accelerating voltage of 20 keV. The as-cast samples were sectioned and polished to 1μm finish and etched with alcoholic ferric chloride. Microstructural images were acquired with secondary electron images. For fracture sections, tensile fracture sections were washed in ethanol in an ultrasonic bath. The true fracture area of fractured samples were obtained with measurement tools on the SEM software. Energy-dispersive X-ray spectroscopy (EDS) attached to the microscope was used to identify microstructural components.

2.6 Small-angle neutron scattering (SANS) and ultra-small-angle neutron scattering (USANS) investigation

Both SANS and USANS experiments were conducted with the OPAL reactor at the Australian Nuclear Science and Technology Organisation (ANSTO), Australia. SANS experiments were carried out in the instrument named QUOKKA [21] which is a 40 m monochromatic pinhole SANS instrument. Three detector distances 1.3 m (with 300 mm offset and 12 m collimation), 12 m (with 12 m collimation), and 20 m (with lens optics 20 m collimation) were used with two different incident neutron beam wavelengths of 5 Å and 8.1 Å (only for 20 m lens optics). The scattering vector (Q) is measured as a function of scattering angle (θ) and the wavelength (λ) as per the following equation:

$$Q = \frac{4\pi \sin\theta}{\lambda}.$$

The range of scattering vector was 7×10^{-4} Å^{-1} to 0.7 Å^{-1}. The appropriate instrument background and sample background was subtracted from the raw data and then data were converted to absolute scale using an empty beam flux as a standard. USANS experiments were conducted at the instrument called KOOKABURRA [22] which extended the Q range up to 2.78×10^{-5} Å^{-1} for the wavelength of 2.37 Å with a resolution (Δλ/λ) of 4%. The data were de-smeared using NIST macros. SANS and USANS data were then combined using IGOR macros [23].

3 Results and discussions

3.1 Thermal and microstructural analysis

To follow the effect of Bi on the thermal behaviour of the solder alloy, DSC was conducted. The melting temperature is critical to the selection of the solder alloy and a vital consideration for improving solder properties. The thermograms obtained from DSC were analysed using a linear baseline to determine the onset of melting during the heating cycle. This allowed the observation of the effect of Bi concentrations on the thermal properties of the Bi-containing SAC series. Figure 4 shows the general effect of Bi substitution on the DSC melting curve. It is seen that for the Bi-free eutectic alloy the melting onset was about 220 °C which is consistent with other published results [24, 25] which reported an equilibrium melting temperature of 217 °C. The slight departure of 2 °C is the result of heating rate dependent superheating under the dynamic DSC heating.

The heating curve was altered by the Bi additions resulting in a widening of the melting peaks and reduced onset temperatures. The use of Bi to reduce the melting temperature has been widely reported [2, 3]. The thermal curve for the eutectic alloy represents freezing into a 3-phase eutectic microstructure.

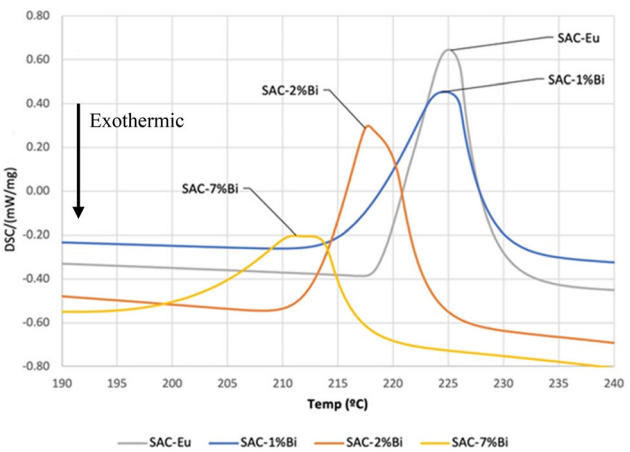

Fig. 4 The effects of Bi substitution for Sn on DSC melting thermograms in the SAC alloy

The dynamic nature of the DSC heating imposes some broadening on the phase changes, however, increases in the broadening of DSC peaks with increasing Bi concentration may be associated with off-eutectic melting. The melting characteristics can be monitored by following the shape of the thermal curves in Fig. 4 for changes that signify changes in the solidification sequence associated with off-eutectic solidification in the Bi-containing alloys. The trend for the reduction in onset temperature with increasing Bi is shown in Fig. 5. The melting range gives further information on the alloy solidification paths.

In the case of eutectic SAC with Bi additions, endothermic peak broadening is observed to remain relatively low (10 – 12 °C) over the Bi concentration range of 0.8–3.0 wt%. Figure 6 shows the changes in peak broadening indicated as DT_R. The small changes in DT_R observed at the concentration range of 0.8–3.0 wt% Bi are thought to be due to the solidification reaction close to the eutectic with the Bi held in solid solution in the b-Sn matrix phase. The broadening of the curve is also followed by examining the full width half maximum (FWHM) per weight for the melting reaction in Fig. 7. A typical ternary eutectic microstructure is shown in Fig. 8 and a schematic depiction of the phase morphologies is presented in Fig. 9. The microstructure consists primarily of b-Sn containing intermetallic phases of Ag_3Sn and Cu_6Sn_5. Previously, it was shown [14] by XRD that established primary Bi precipitates can only be detected at Bi concentrations greater than 3%, hence SEM examinations of SAC with lower Bi content present similar microstructures to that of the eutectic. However, beyond the Bi solubility limit further broadening of the DSC melting peaks can be attributed to the formation of a pro-eutectic primary phase of Bi which

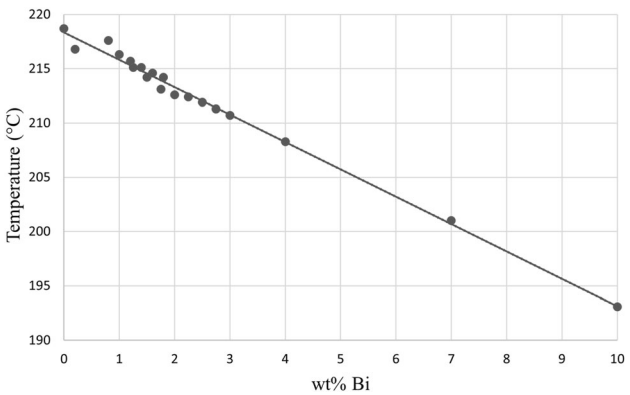

Fig. 5 Onset melting temperature of eutectic SAC-Bi (0–10%wt)

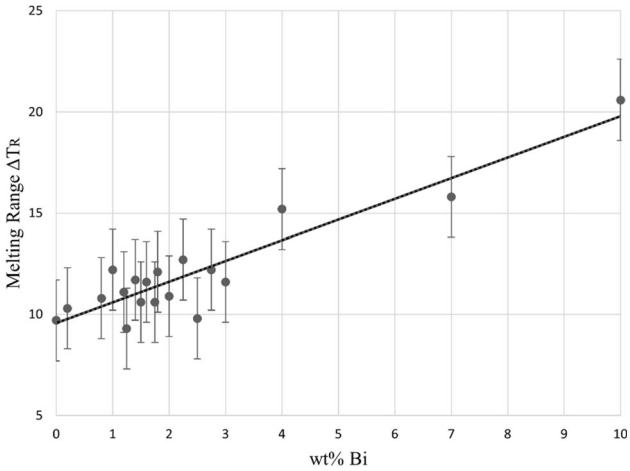

Fig. 6 Effect of Bi substitution (0–10 wt% Bi) on DSC melting range ΔTR °C

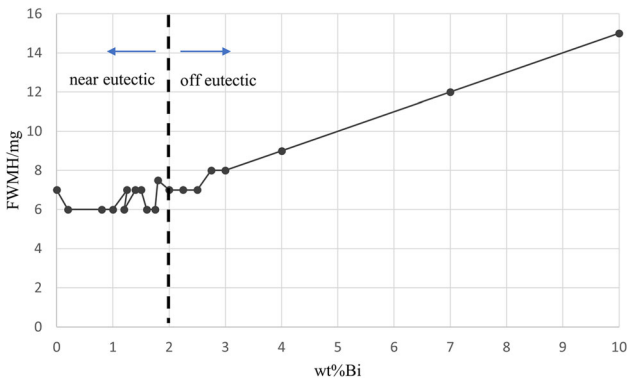

Fig. 7 Full width half maximum (FWHM) per weight for the melting reaction (0–10 wt% Bi)

is well distributed throughout the matrix phase as fine precipitates during solidification [26]. The large DT_R observed for alloys with greater than 3% Bi clearly indicates off-eutectic melting in conjunction with the well-established formation of the primary Bi-phase in the microstructure.

The solidification behaviour of the solder and its microstructure is affected by the degree of undercooling which is characterised as $\Delta T = T_L - T_S$, where T_L is the temperature during the heating stage at which the melting starts, and TS is the temperature during the cooling stage at which solidification occurs. The degree of undercooling can therefore be determined by comparing the difference between each onset temperature in the heating and cooling curve. Alloying elements into solder alloys provide additional nucleation sites which promote the solidification process [26]. To achieve refinement in the

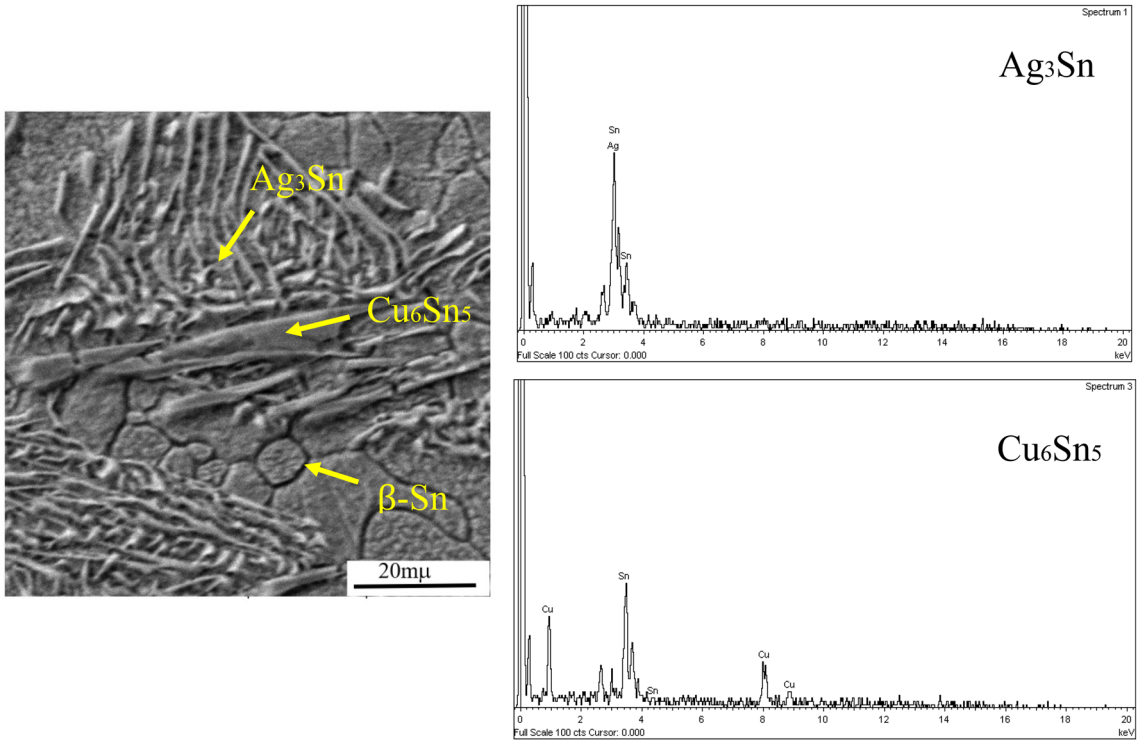

Fig. 8 Typical microstructure of SAC with 3-phase eutectic of β-Sn, Ag3Sn, and Cu6Sn5 (left); and EDS spectra identifying Cu6Sn5 and Ag3Sn (right)

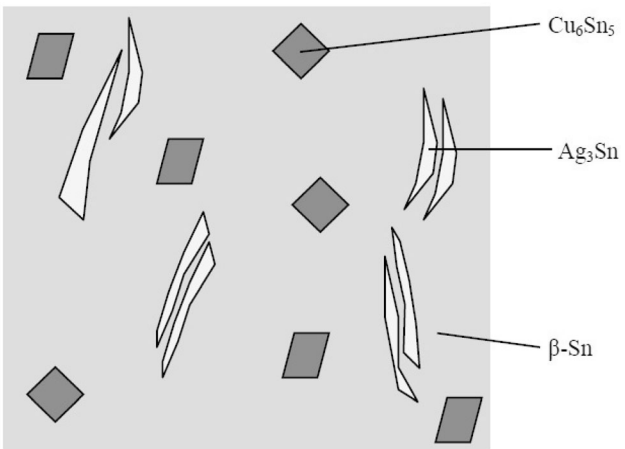

Fig. 9 Schematic illustration showing morphology of intermetallic compounds of Cu6Sn5 and Ag3Sn

microstructure and better heterogeneous nucleation of solidified phases a reduction in undercooling is desired. As shown in Fig. 10 the addition of bismuth to the SAC solder reduces the degree of undercooling which can lead to improvement through refining the microstructure of the solder alloy. The lower degree of undercooling favours better nucleation of solidified phases through heterogeneous nucleation at Bi particles [27]. The finer microstructure is attributed to a faster solidification rate for the Ag_3Sn and β-Sn phases which leads to an increase in the availability of heterogeneous nucleation sites for the primary IMCs [26–28]. The evolution of microstructure that is associated with the solidification path is expected to influence on the mechanical properties of the different solder compositions.

3.2 Mechanical properties

The mechanical properties of the Bi-containing SAC alloys were evaluated using standard tensile tests. The stress–strain curves typifying the effects of Bi on the mechanical properties of the SAC alloy is shown in Fig. 11. The ultimate tensile strength (s_u) was 50 MPa for ternary SAC and increases with Bi to a maximum of 90 MPa for 10% Bi substitution. The modulus of elasticity (E) obtained from tensile test results was 48 – 50GPa and did not follow any clear trend with Bi content. The non-varying trend in E with %Bi is because the elastic property is fundamentally related to metallic bonding offered by the β Sn and this is not a microstructure sensitive property. It is evident that there was a reduction in ductility

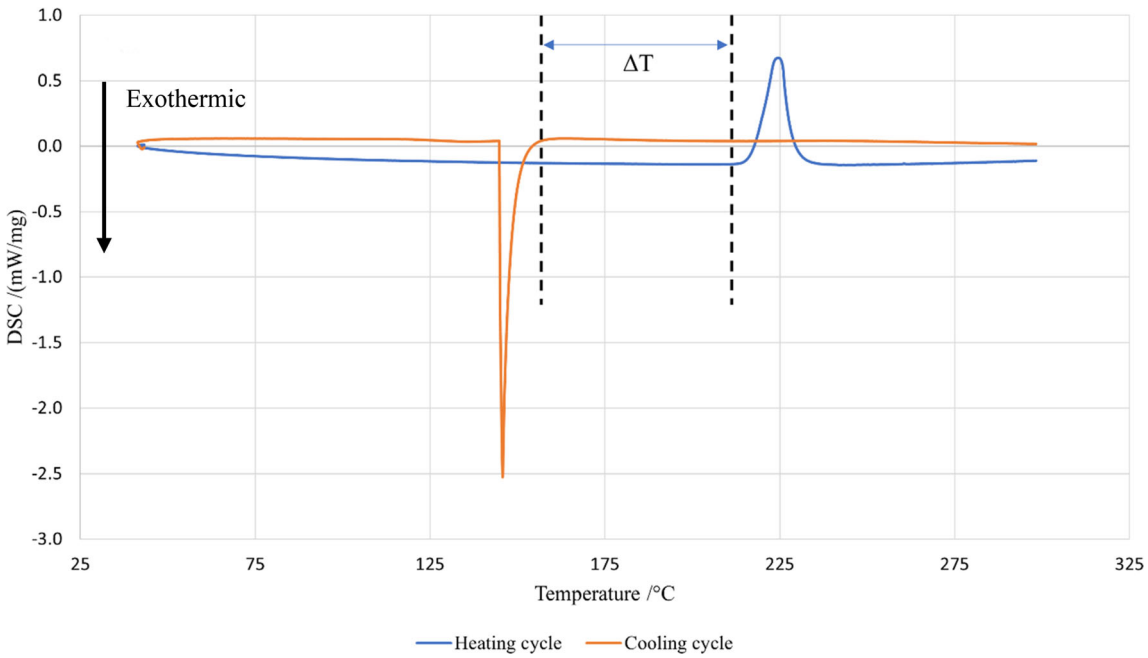

Fig. 10 DSC heating and cooling curves of solder alloy SAC-0.8Bi showing extent of undercooling (ΔT)

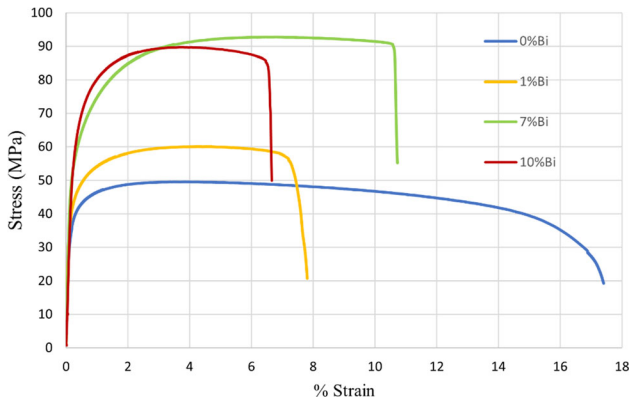

Fig. 11 Effects of Bi substitution in SAC on the stress–strain data obtained from tensile tests

with increasing levels of Bi substitution as shown in Fig. 12 which presents the derived mechanical properties from the stress–strain curves as a function %Bi in SAC. The fracture strain was about 17% for SAC and drastically dropped to less than 10% for concentrations with more than 1% Bi. Figure 13 shows the difference in reduction in the area with varying compositions of Bi. The observed reductions in ductility with increasing Bi are highlighted by the clear difference in reduction in the area after fracture, in Fig. 14, for the SAC alloy containing 7 wt% Bi versus the Bi-free alloy.

Ismuth is intrinsically brittle and the SAC with high Bi concentrations forms Bi precipitates in the β-Sn matrix by proeutectic reaction which lead to reduced ductility. At lower Bi levels (less than 5 wt%) growth of intermetallic compounds is limited, and fine precipitates of Bi form during cooling in the Sn solid solution which increases the strength of the solder matrix. These fine precipitates have stable chemical bonding and impede dislocation movement causing increases in strength and a decrease in ductility of the alloy [26]. The ultimate tensile strength (s_u) and yield strength (s_y) obtained from the 0.2% offset method as a function of %Bi in SAC can be observed in Fig. 12. Both s_y and s_u follow the same trend. It is seen that s_u increased from 50 to 60 MPa at dilute concentration of Bi in SAC up to 1.8 wt% Bi without drastic loss in ductility indicated by elongation at fracture. The effect of Bi in increasing strength plateaued at 60 MPa between Bi concentrations of 1.8 – 2 wt% Bi and in this concentration range there was a dramatic drop (approximate 50%) in ductility to 10 – 15% in elongation at fracture. The initial effect of Bi in increasing the strength at the low Bi content (< 2% Bi) can be attributed to solid solution strengthening. This is in accordance with results from DSC thermal analyses (Figs. 4, 5, 6) that supports that SAC-Bi in this concentration range undergoes near-eutectic melting/solidification for which

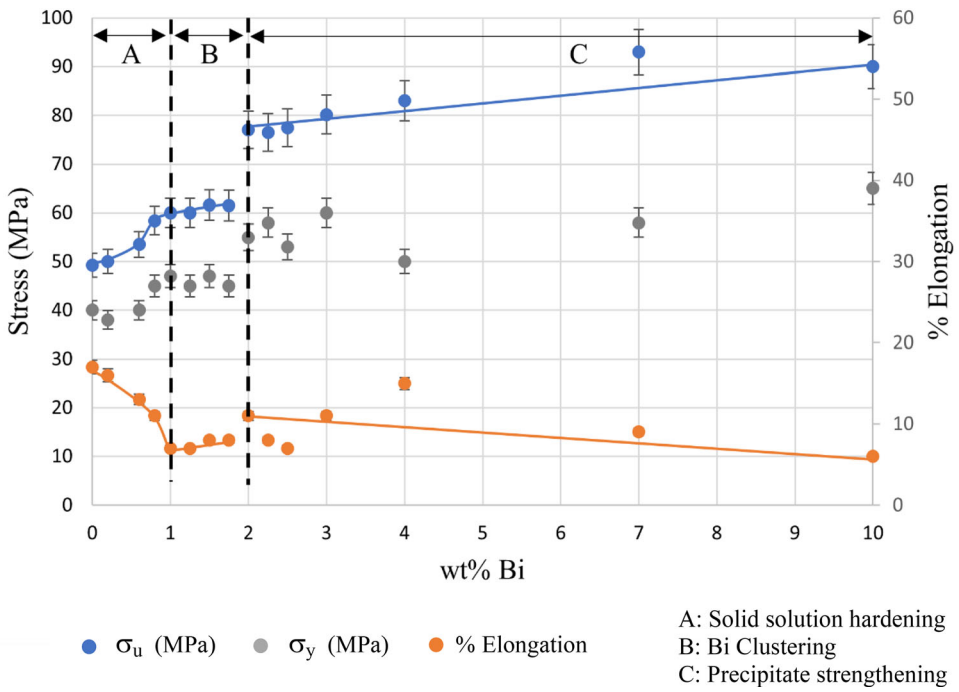

Fig. 12 Mechanical properties derived from tensile tests

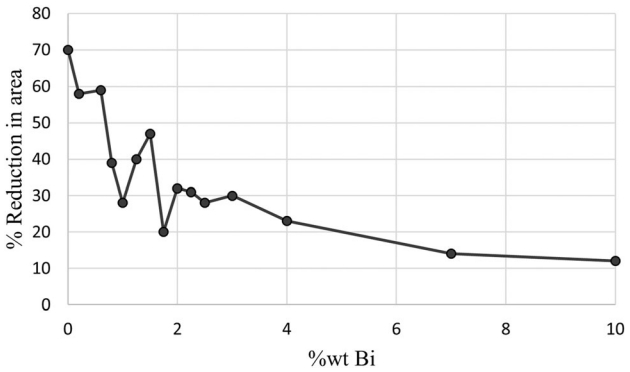

Fig. 13 Effects of Bi substitution in SAC on the reduction in area obtained from tensile tests

there were no hardening effects from a primary pro-eutectic Bi-phase. However, the rapid loss of ductility observed at concentration range 1.5–2 wt% Bi suggests the possibility of a fine-scale, i.e. below the resolution able to be observed under SEM, microstructural event which has led to the embrittlement. The EDS results (Fig. 8) confirmed the existence of established primary Bi precipitates at 3 wt% Bi in eutectic SAC. However, evidence from both mechanical and thermal analyses suggest that the limit of solid solubility lies at a more dilute Bi concentration. This was further investigated with Neutron Scattering methods using Small angle and Ultra-

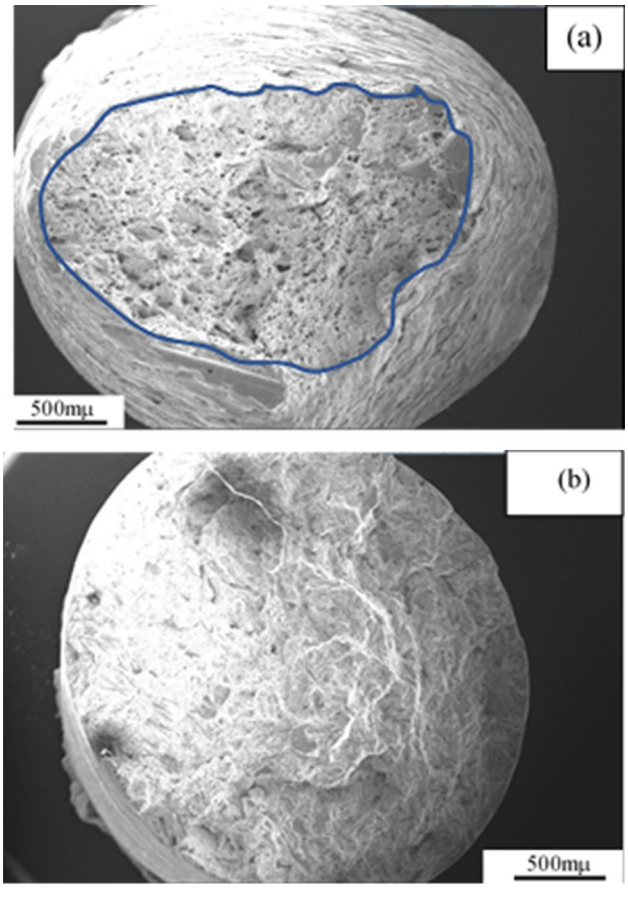

Fig. 14 Fractographic images of **a** Eutectic SAC with large reduction in area, **b** SAC-Eu-7%wt Bi

small angle (SANS and USANS) in the following section.

The strength of alloys containing 2 wt% Bi was 80 MPa and increased gradually reaching 90 MPa at 10% Bi. There was no further deterioration in ductility with higher Bi contents. The effects observed for SAC-Bi with more than 2% Bi can be attributed to the precipitate hardening arising from the effects of established primary Bi precipitates. This is consistent with thermal analyses that support the off-eutectic behaviour of alloys in this Bi concentration range.

3.3 Small-angle neutron scattering (SANS) and ultra-small-angle neutron scattering (USANS)

For the SAC-Bi compositions in the range of 0.8–2.0 wt% Bi near the limits of the Bi solid solubility, due to the observed mechanical behaviour where there was a loss of ductility in conjunction with differences detected via thermal analyses, samples around this compositional range were subjected to (ultra) small-angle neutron scattering experiments. The data for scattering were obtained using separate instruments for SANS and USANS to obtain scattering data for a wide range of scattering factor Q from 2.78×10^{-5} Å^{-1} to 0.7 Å^{-1}. The scattering factors (Q) for SAC-Bi of 0.8–2.75 wt% Bi are presented in Figs. 15 and 16. For high Q ranging from $10^{0} - 10^{-2}$Å^{-1}, some changes can be observed at 5×10^{-2}Å^{-1} corresponding to a length scale of 12.5 nm. However, from Q slightly below 10^{-2}Å^{-1}, for the 0.8 wt% Bi concentration the scattering intensity is significantly lower than for the other compositions as we approach a scattering factor around 10^{-4}Å^{-1}. The scattering for the 0.8 and 1.5 wt% Bi samples were distinct from that of the higher Bi (2 and 2.75 wt% Bi concentrations) which were coincident. The changes in the scattering behaviour indicate that a nano-scale microstructural clustering phenomenon occurs in the composition range of 1.5–2 wt% Bi which is likely the cause of the observed loss in ductility as well as the differing thermal behaviours for these compositions. The Q value of 10^{-2}Å^{-1}, where this change in scattering becomes evident translate to a length scale of 10 to 100 nm. Since for higher concentrations of Bi (> 2 wt% Bi), the existence of established Bi precipitates which contribute to hardening is not in doubt, it is proposed that the nanometric length scale differences in scattering could be due to the presence of precursor Bi clusters that were responsible for observed embrittlement in the concentration range beyond the solid solubility limit (1.5 wt% Bi) and up to the concentration when distinct Bi precipitates form (2 wt% Bi).

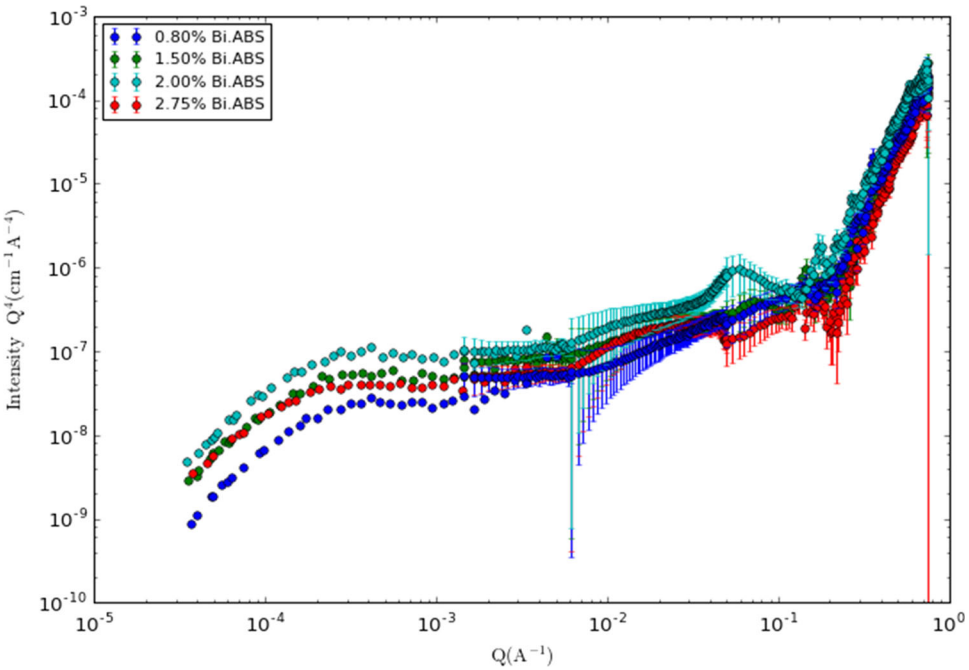

Fig. 15 SANS and USANS experiments data plot

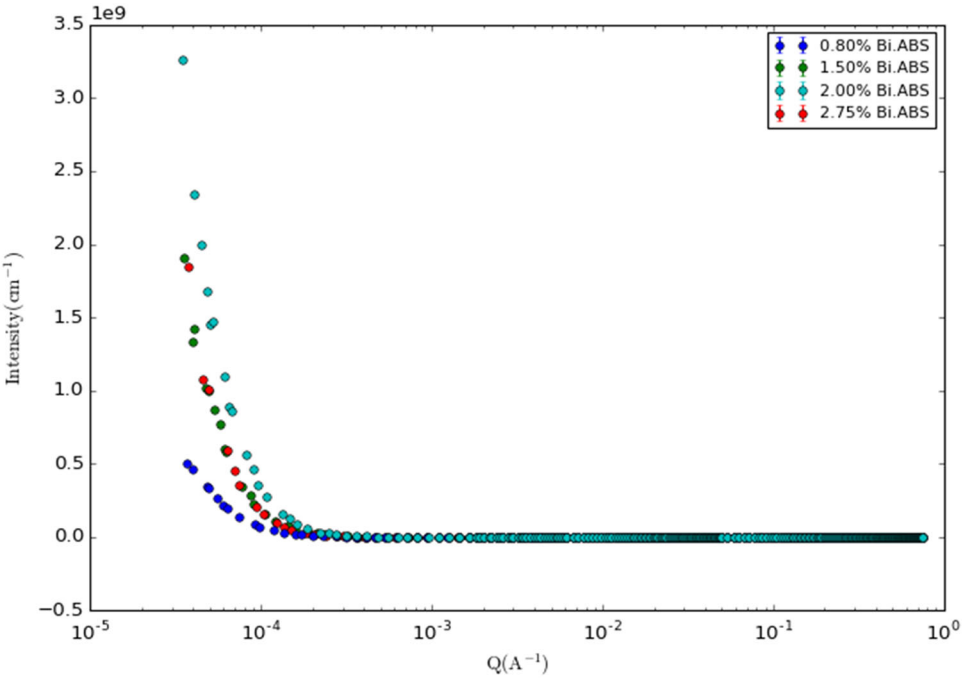

Fig. 16 SANS and USANS experiments data plot

4 Outlook for application of Bi-containing SAC solders

The development of Pb-free solders which mimic the operational properties of classic SnPb eutectic solders is becoming increasingly vital for the microelectronics industry. However, forming effective Pb-free solders is challenging and further metallurgical insight to advance the current understanding of ternary and quaternary Pb-free solder systems is required until the technology can fully step away from the binary SnPb solder of the past. Due to their resemblance to SnPb solders and high electrical and mechanical performance, SAC eutectic (Sn3.5Ag0.9Cu) and near-eutectic (SAC305/405) alloys are perhaps the leading alternatives. Extensive research on SAC solders with varying compositions of Ag pertains to reducing the contents of the high-cost Ag component and hence improve overall solder affordability. SAC solders with low Ag content (< 3 wt%) which have been alloyed with traces of Rare Earth elements like Pr, Ga, Ce, Nd, and Dy have proven effective in enhancing wettability and mechanical properties but show deterioration in properties with increasing concentrations. [28–31] The alloying elements in the solder alloy lower the diffusion coefficient resulting in the formation of thinner IMCs which results in a stronger joint [32]. In recent literature SAC (257) solder with the addition of Bi in weight percentages up to 5 wt% showed that Bi greatly affects the mechanism of formation of IMCs in the solder during solidification hence refining the microstructure whilst imparting strength to the alloy and lowering the melting temperature [33]. In other work, SAC (157) with the addition of 3 wt% Bi has shown higher creep resistance and improved creep lifetime compared with the base solder [26]. Bi has been reported to restrict tin whisker growth in SAC-Bi alloy [1].

Our preliminary research [14] indicated that the maximum Bi content for lowering the processing temperature of eutectic SAC alloys should be below 2 wt% but there was still a need to develop further understanding on the role of Bi on the solder properties and also on the impacts of higher levels of Bi which has motivated this research. Building on this prior work, we have observed that Bi clustering in the 1.5–2 wt% Bi composition range, which is below the concentration at which discrete Bi precipitates have been detected to form, causes embrittlement of the alloy. This hitherto undetected phenomenon has important implications for the formulation of robust and long-lasting SAC-Bi solder joints. Additionally, increasing Bi contents in SAC-Bi solder beyond 2 wt% promoted increases in strength peaking at 7 wt% Bi at 93 MPa, nearly twice that of eutectic SAC alloy whilst still maintaining substantial (> 10%) ductility. Despite the reduced ductility at this higher Bi content, the alloy has superior strength which will serve

for more efficient component handling, logistics, and durability. The findings of this research indicate that there is substantial potential to further understand the full effect of Bi in solder applications, particularly for targeted applications. Therefore, the opportunity to study and compare creep models, wettability and biomedical behaviour of eutectic SAC alloy with varying Bi concentrations is presented.

5 Conclusion

In this study substitution of Bi for Sn in a eutectic SAC solder was investigated. The Bi was shown to alter the solidification path and mechanical properties of SAC related to its influence on the eutectic reaction. Generally, the onset for melting decreases with increasing Bi concentrations dropping from 217 °C to around 193 °C for 10% Bi substitution. The tensile strength for ternary SAC is 50 MPa and increases with Bi content to 60 MPa plateauing at between 1.4 and 1.8 wt% Bi. The increase was associated with solid solution strengthening imparted by Bi to the β-Sn matrix. Tensile tests indicated that at between 1.4 and 2 wt% Bi samples became brittle with a smaller reduction in area and substantially reduced strain at fracture. Neutron scattering experiments suggested that in this concentration range, there was evidence of atomic (Bi) clustering at a scale in the range of 10–100 nm. The DSC studies indicated that off-eutectic reaction led to the formation of primary Bi precipitates at concentrations higher than 2 wt%. The outcome of this work suggests that the use of Bi modification of SAC as an electrical interconnect material provided increased joint strength and a lower processing temperature. The increased strength and lower melting temperatures must be balanced against the loss of ductility and this work should inform practice in designing SAC alloys to suit various functional requirements in electronic devices designed to meet RoHS compliance.

Acknowledgements

The authors acknowledge AINSE for awarding grant No. 8285 to carry out neutron diffraction studies at ANSTO.

Authors' Contributions

AO, RH, and DK were responsible for project conceptualization. AO, RH, and LS carried out all laboratory tests and developed methodology. Nuclear Scattering experiments including interpretation of results by JM, RH, and DK. MR, and LS contributed to writing—original draft preparation, AO, DK, and RH carried out the review and editing. All authors have read and agreed to the published version of the manuscript.

Funding

The neutron scattering studies reported in this work was carried out at Australian Nuclear Science and Technology Organisation (ANSTO), funded with AINSE grant No. 8285.

Data Availability

Not Applicable.

Code availability

Not Applicable.

Declarations

Conflicts of interest The authors have no conflict of interest.

Ethics approval Not Applicable.

Consent to participate All authors consent to participate in this work.

Consent for publication All authors have consented to the publication of this work.

References

1. S. Cheng, C.-M. Huang, M. Pecht, Microelectron. Reliab. **75**, 77 (2017)
2. X. Hu, Y. Li, Y. Liu, Z. Min, J. Alloy. Compd. **625**, 241 (2015)
3. J. Shen, Y. Pu, D. Wu, Q. Tang, M. Zhao, J. Mater. Sci.: Mater. Electron. **26**, 1572 (2015)

4. R. Coyle, J. Osenbach, M.N. Collins, H. McCormick, P. Read, D. Fleming, R. Popowich, J. Punch, M. Reid, S. Kummerl, IEEE Trans. Compon. Packaging Manuf. Technol. **1**, 1583 (2011)
5. M.N. Collins, J. Punch, R. Coyle, M. Reid, R. Popowich, P. Read, D. Fleming, IEEE Trans. Compon. Packaging Manuf. Technol. **1**, 1594 (2011)
6. M.E. Loomans, M.E. Fine, Metall. Mater. Trans. A **31**, 1155 (2000)
7. E. Dalton, G. Ren, J. Punch, M.N. Collins, Mater. Des. **154**, 184 (2018)
8. K.-W. Moon, W.J. Boettinger, U.R. Kattner, F.S. Biancaniello, C.A. Handwerker, J. Electron. Mater. **29**, 1122 (2000)
9. S. Zhang, X. Xu, T. Lin, P. He, J. Mater. Sci.: Mater. Electron. **30**, 13855 (2019)
10. S. Li, X. Wang, Z. Liu, J. Yongtao, Z. Shuye, G. Jinfeng, X. Chen, W. Shengjin, P. He, W. Long, J. Mater. Sci.: Mater. Electron. **31**, 9076 (2020)
11. M.L. Huang, L. Wang, Metall. and Mater. Trans. A. **36**, 1439 (2005)
12. D. Witkin, J. Electron. Mater. **41**, 190 (2012)
13. X. Hu, Y. Li, Y. Liu, Z. Min, J. Alloys Compd. **625**, 241 (2015)
14. A. Olofinjana, R. Haque, M. Mathir, N.Y. Voo, Procedia Manuf. **30**, 596 (2019)
15. G. Ren, I.J. Wilding, M.N. Collins, J. Alloys Compd. **665**, 251 (2016)
16. C.-B. Lee, S.-B. Jung, Y.-E. Shin, C.-C. Shur, Mater. Trans. **43**, 1858 (2002)
17. Y.-W. Yen, C.-C. Jao, C. Lee, J. Mater. Res. **21**, 2986 (2006)
18. T. Laurila, J. Hurtig, V. Vuorinen, J.K. Kivilahti, Microelectron. Reliab. **49**, 242 (2009)
19. I.E. Anderson, A. Boesenberg, J. Harringa, D. Riegner, A. Steinmetz, D. Hillman, J. Electron. Mater. **41**, 390 (2012)
20. A.S. Basin, A.B. Kaplun, A.B. Meshalkin, N.F. Uvarov, Russ. J. Inorganic Chem. **53**, 1509 (2008)
21. K. Wood, J.P. Mata, C.J. Garvey, C.-M. Wu, W.A. Hamilton, P. Abbeywick, D. Bartlett, F. Bartsch, P. Baxter, N. Booth, W. Brown, J. Christoforidis, D. Clowes, T. d'Adam, F. Darmann, M. Deura, S. Harrison, N. Hauser, G. Horton, D. Federici, F. Franceschini, P. Hanson, E. Imamovic, P. Imperia, M. Jones, S. Kennedy, S. Kim, T. Lam, W.T. Lee, M. Lesha, D. Mannicke, T. Noakes, S.R. Olsen, J.C. Osborn, D. Penny, M. Perry, S.A. Pullen, R.A. Robinson, J.C. Schulz, N. Xiong, E.P. Gilbert, J. Appl. Crystallogr. **51**, 294 (2018)
22. C. Rehm, L. de Campo, A. Brûlé, F. Darmann, F. Bartsch, A. Berry, J. Appl. Crystallogr. **51**, 1 (2018)
23. S.R. Kline, J. Appl. Crystallogr. **39**, 895 (2006)
24. F.X. Che, J.H.L. Pang, J. Alloys Compd. **541**, 6 (2012)
25. H.R. Kotadia, P.D. Howes, S.H. Mannan, Microelectron. Reliab. **54**, 1253 (2014)
26. R. Sayyadi, H. Naffakh-Moosavy, Sci. Rep. **9**, 8389 (2019)
27. A.A. El-Daly, W.M. Desoky, A.F. Saad, N.A. Mansor, E.H. Lotfy, H.M. Abd-Elmoniem, H. Hashem, Mater. Des. **80**, 152 (2015)
28. A.A. El-Daly, A.M. El-Taher, S. Gouda, J. Alloys Compd. **627**, 268 (2015)
29. H. Wang, S. Xue, J. Wang, J. Mater. Sci.: Mater. Electron. **28**, 8246 (2017)
30. J. Xu, S. Xue, P. Xue, W.-M. Long, Q.-K. Zhang, J. Mater. Sci.: Mater. Electron. **27**, 8771 (2016)
31. H. Chen, J. Liao, S. Wu, L. Gong, J. Wang, H. Wang, J. Mater. Sci.: Mater. Electron. **29**, 12662 (2018)
32. E.E.M. Noor, A. Singh, Soldering & Surface Mount Technology **26**, 147 (2014)
33. R. Sayyadi, H. Naffakh-Moosavy, Mater. Sci. Eng., A **735**, 367 (2018)